Mathematical Biosciences and Engineering

MBE, 20(10): 17849–17865.
DOI: 10.3934/mbe.2023793
Received: 29 July 2023
Revised: 04 September 2023
Accepted: 11 September 2023
Published: 18 September 2023

http://www.aimspress.com/journal/MBE

Research article

Effect of the electromagnetic induction on a modified memristive neural map model

Prasina Alexander[1], Fatemeh Parastesh[2], Ibrahim Ismael Hamarash[3,4], Anitha Karthikeyan[5,6], Sajad Jafari[2,7] and Shaobo He[8,*]

[1] Centre for Nonlinear Systems, Chennai Institute of Technology, Chennai, India
[2] Department of Biomedical Engineering, Amirkabir University of Technology (Tehran Polytechnic), Iran
[3] Electrical Engineering Department, Salahaddin University-Erbil, Kirkuk Rd., Erbil, Kurdistan, Iraq
[4] School of Computer Science and Engineering, University of Kurdistan Hewler, 40m St., Erbil, Kurdistan, Iraq
[5] Department of Electronics and Communication Engineering, Vemu Institute of Technology, Chithoor, India
[6] Department of Electronics and Communications Engineering and University Centre for Research & Development, Chandigarh University, Mohali-140413, Punjab
[7] Health Technology Research Institute, Amirkabir University of Technology (Tehran Polytechnic), Iran
[8] School of Automation and Electronic Information, Xiangtan University, Xiangtan 411105, China

* **Correspondence:** Email: heshaobo_123@163.com.

Abstract: The significance of discrete neural models lies in their mathematical simplicity and computational ease. This research focuses on enhancing a neural map model by incorporating a hyperbolic tangent-based memristor. The study extensively explores the impact of magnetic induction strength on the model's dynamics, analyzing bifurcation diagrams and the presence of multistability. Moreover, the investigation extends to the collective behavior of coupled memristive neural maps with electrical, chemical, and magnetic connections. The synchronization of these coupled memristive maps is examined, revealing that chemical coupling exhibits a broader synchronization area. Additionally, diverse chimera states and cluster synchronized states are identified and discussed.

Keywords: neural map model; memristive map; bifurcation; synchronization; chimera state

1. Introduction

Discrete models, also known as discrete maps, serve as mathematical representations to describe how a system evolves at specific time intervals [1]. In contrast to continuous models that employ differential equations to describe a system's behavior over time continuously, discrete maps use iterative equations. The simplicity of discrete models, owing to the absence of calculus or differential equations, makes them more accessible for comprehension, implementation, and analysis [2]. Their computational efficiency allows them to need fewer computational resources than solving intricate differential equations. These discrete models have many applications in diverse scientific and engineering fields. They can be used to study population dynamics [3], such as animal population growth and infectious disease spread, as well as in economic and financial systems [4,5]. Moreover, discrete maps can be used for exploring chaotic behavior in various systems wherein simple equations can yield unpredictable and intricate trajectories [6,7].

Discrete models have offered valuable insights into the dynamic behavior of neural networks [8]. The simplicity of discrete models makes them suitable for understanding the complex interactions and dynamics of neural networks. These models facilitate investigation of various cognitive functions, sensory processing, and information propagation within the brain [1]. By discretely representing neural activity, researchers can analyze complex neural phenomena with more efficiency, leading to a deeper understanding of network behaviors. One significant application of discrete models in neuroscience is the study of synchrony and collective patterns in networks [9–12]. For example, Bashkirtseva et al. [10] studied the synchronization in the map-based Chialvo neuron model and reported a critical noise value for the synchronization of neurons. Sausedo-Solorio [11] studied the synchronization of Rulkov neurons with memory and synaptic delay. They found that anticipation or lag synchronization may emerge relying on delay time. Moreover, discrete models have been used for exploring phenomena such as neural firing patterns and synaptic plasticity [13–15]. For example, He et al. [14] described a new discrete neuron model based on the Huber-Braun neuron and discussed the effects of temperature-dependent ion channels on the firing patterns. Wang et al. [15] analyzed the dynamics of a discrete-time Chialvo neuron model through bifurcation diagrams and Lyapunov exponents.

The discovery of the fourth electrical component, named memristor, has led many scientists to modify the existing dynamical system or suggest new systems [16]. As a result, numerous memristive continuous or discrete time systems have been introduced with various distinctive features, such as amplitude control [17,18]. Incorporating memristor in neural models helps reproduce the neural behaviors more accurately [19]. The memristor is an electrical component connecting the charge and magnetic flux [20,21]. Therefore, it can be used for considering the effects of electromagnetic induction [22]. The variation of neurons' membrane voltage can change the distribution of the electromagnetic field around the membrane, which significantly impacts the neuron's activities. Moreover, the memristors have memory, making them suitable for modeling the synaptic strengths of biological neurons [23]. The synaptic connections play a crucial role in information processing and learning [24]. Consequently, the neural network models have been improved using the memristor [25,26].

Several researchers have explored the effect of memristors on neuron models [27]. Xu et al. [28] introduced a 3D memristor-based Wilson neuron model that could represent asymmetric coexisting electrical activities and antimonotonicity. Qiao and Gao [29] used a Filippov-type Wilson neuron model to examine the effect of temperature and magnetic induction. They presented a complete analysis on the model by applying multiple nonlinear dynamic tools. Li et al. [30] represented different

coexisting periodic and chaotic attractors in the memristive Hindmarsh-Rose model. Lai et al. [31] proposed a new memristive neuron model with special chaotic properties and showed its application in image encryption. Gao et al. [32] improved a four-dimensional Filippov Hindmash-Rose with considering a memristive autapse with the threshold control strategy, which could cause the occurrence of sliding bursting, sliding limit cycle and coexisting attractors. In another study [33], they applied the analysis on a 4D Filippov hybrid neuron model and found the local stability and bifurcation conditions.

The presence of memristors in neural networks can also influence their collective behaviors. Synchronization is the most important behavior in complex networks [34–36]. Hence, a large number of studies have been devoted to the study of synchronization in memristive neural networks [37–39]. Besides, other partial synchronization patterns, such as chimera state [40,41] and cluster synchronization [42,43], have special associations with neural processes [44]. Li et al. [45] studied the synchronization of two Rulkov maps coupled with a memristor synapse and showed complete and lag synchronization behaviors. Ramakrishnan et al. [46] found different collective behaviors such as imperfect synchronization, solitary state, cluster synchronization, and chimera states in coupled memristive neuron maps. Wang et al. [47] investigated the synchronization of memristive HR maps with electrical synapses, chemical synapses, inner linking functions, and hybrid synapses. They found that coupled maps could get synchronized via electrical and mixed synapses.

In this paper, we investigate the effects of electromagnetic induction on the dynamics of a neural map model by adding the memristor to the model. The considered neural map model is a behavioral model proposed based on some physiological facts about the attention control mechanism and chaos intermittency. The model's coefficients are related to the brain synapses' weights regulated by the release of different neurotransmitters. Analyzing this model can help recognize inhibitory problems in people with Attention Deficit Disorder. Motivated by previous studies that suggest the advantages of memristors on neuron and neural models, we study this model with a memristor. We consider its dynamics under magnetic induction, which can help in studying the alternation of attention levels in different cases. To this aim, the bifurcation diagrams are plotted for different magnetic induction strengths and the dynamics is considered. The impact of the initial conditions and the coexisting dynamics is also explored. Besides the single map model, the dynamical behavior of coupled memristive neural maps is studied by applying different synapses such electrical, chemical and magnetic couplings. Various network patterns such the synchronization, cluster synchronization and chimera states are shown.

2. Model

We consider a discrete neural model, which was introduced by Baghdadi et al. in 2015 [48]. This model is described as follows,

$$x(n+1) = B\tanh(w_1 x(n)) - A\tanh(w_2 x(n)) \tag{1}$$

where A, B, w_1, and w_2 are the parameters by adjusting which the model represents a variety of dynamical behaviors. By setting $B = 5.821$, $w_1 = 1.487$, $w_2 = 0.2223$, the bifurcation diagram according to A is shown in Figure 1(a). It should be noted that the system has coexisting attractors in some values of the parameter A. In this figure, the red and blue colors correspond to the negative and positive initial conditions, respectively.

A voltage-controlled memristor is generally described as,

$$i_M = W(\phi)v_M \tag{2}$$

where i_M is the electromagnetic induction current, v_M is the neuron's membrane potential, and $W(\phi)$ is the memristor memductance function. The neuron's activation function is monotonically differentiable and bounded above and below. Hence, the hyperbolic tangent function has been widely used as the neuron's activation function [49–51]. Therefore, $W(\phi) = \tanh(\phi)$.

The discrete model for the memristor can be obtained by applying the continuous discretization method to the continuous flux-controlled memristor models. A discrete memristor model was presented by [52] as,

$$i(n) = W\big(\phi(n)\big)v(n) = \tanh\big(\phi(n)\big)\, v(n) \tag{3}$$

$$\phi(n+1) = \phi(n) + \varepsilon v(n)$$

where ϕ is the flux variable and v and i are the memristor's voltage and current. More details about this memristor and its fingerprints can be found in [52]. Since the memristor contains nonlinearity and possesses memory effects, it complies with real memristive properties and can be used for the representation of more accurate neural dynamics and synaptic plasticity processes.

Using the defined memristor, the memristive neural map model can be defined as,

$$x(n+1) = B\tanh(w_1 x(n)) - A\tanh(w_2 x(n)) + \mu\, x(n)\tanh\big(\phi(n)\big) \tag{4}$$

$$\phi(n+1) = \phi(n) + \varepsilon x(n)$$

where μ is the magnetic induction strength and $\varepsilon = 1$ is set. In the following, we analyze the dynamics of the memristive map model and the collective behavior of coupled memristive maps.

3. Dynamics of the memristive model

The magnetic flux effects through the memristor can considerably influence the model dynamics. The bifurcation diagrams of the memristive model for different magnetic induction strengths (μ), according to the parameter A, are shown in Figure 1(b)–(d). To obtain the bifurcation diagrams the attractor-following method [33,53] is used, where the result of each iteration serves as the initial value of the next iteration. The forward and backward continuations are shown by red and blue colors. Comparing the bifurcation diagrams in presence of memristor with the original model (Figure 1(a)) suggests that as the magnetic flux strengthens, the region of multistability is extended. The coexisting attractors of the main model exist in the range $A < 9.556$ and $A > 24.35$, while in the memristive version, the coexisting attractors are visible for almost all A values as $A > 8.63$ for $\mu = 0.1$, $A > 7.9$ for $\mu = 0.2$ and $A > 7.18$ for $\mu = 0.3$. Therefore, existence of the memristor promote multistability property.

The presence of multiple stable states in multistability can provide different cognitive or perceptual interpretations, and studying the transitions between these states can provide valuable insights into the brain's information processing and behavior generation. An important application of multistability is in understanding perceptual phenomena, where an ambiguous sensory input can cause oscillations between different interpretations [54]. Additionally, multistability is also relevant in decision-making processes, as the coexistence of multiple stable states corresponds to alternative decisions or choices [55]. Another example is the cognitive flexibility in which the brain is able to

switch rapidly between different mental states or cognitive processes [56]. The transition between several stable states helps to the brain's adaptation to varying external demands.

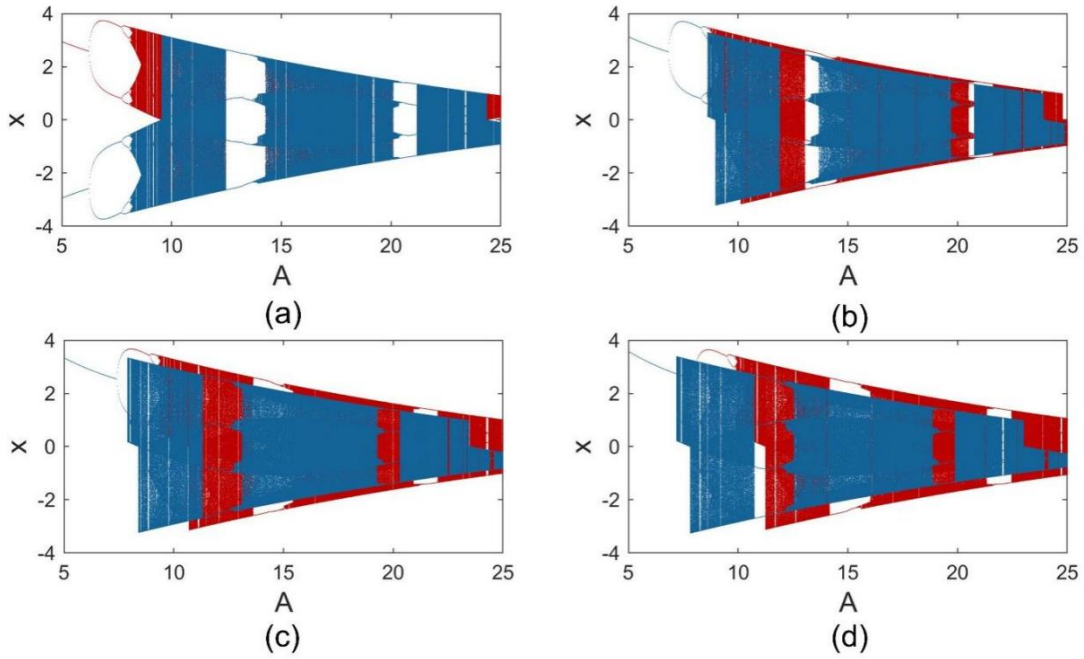

Figure 1. Bifurcation diagrams of the original neural map model (a), and its memristive version (b–d) for different magnetic induction effects as a function of A. (a) $\mu = 0$, (b) $\mu = 0.1$, (c) $\mu = 0.2$, (d) $\mu = 0.3$. The bifurcations are obtained using attractor-following method (forward: red color and backward: blue color) using the initial condition [1,0].

In the following, the dynamics of the memristive model are investigated by setting $A = 8$. Figure 2 shows the bifurcation diagram according to μ. The blue, red, and cyan colors are related to $[-1, 0]$, $[1, 0]$, and $[-5, 4]$, respectively. It is seen that varying μ can considerably change the dynamics of the model. Moreover, the dynamics are highly dependent on the initial conditions. However, the probability of observing periodic dynamics is higher for stronger magnetic induction. The bifurcation diagram obtained by the forward continuation for two initial conditions [1,0] and [-1,0] are shown in Figure 2(b). It is notable that the bifurcation obtained with the fixed initial condition [1,0] is the same as one obtained by its forward continuation. Figure 3 illustrates the dynamics of the original model in $A = 8$ (Figure 3(a)) and $A = 9$ (Figure 3(b)), and its variation under magnetic induction. In parts (a1) and (b1), the response of the original model is depicted where it is periodic in $A = 8$ and is chaotic in $A = 9$. In parts (a2–a4) and (b2–b4), the magnetic induction is $\mu = 0.02$, $\mu = 0.05$, and $\mu = 0.1$, respectively. It is observed that in the case of $A = 8$, adding the memristor can increase the period of time series or induce chaos. Similarly, for $A = 9$, the memristor can change the chaotic dynamics and lead to different periodic behaviors and also different chaotic dynamics. Therefore, the dynamics are considerably affected by the memristor; however, increasing its strength has a different impact and is dependent on the original dynamics.

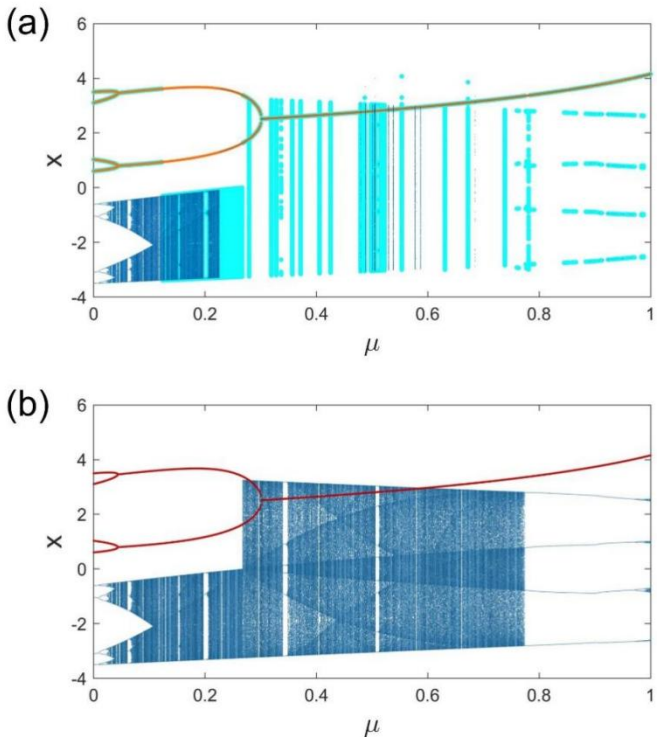

Figure 2. Bifurcation diagram of the memristive neural map model for $A = 8$ as a function of μ. (a) The blue, red and cyan colors correspond to the initial conditions $[-1,0]$ and $[1,0]$, and $[-5,4]$, respectively. (b) The forward continuation is used for the initial condition $[1,0]$ (red) and [-1,0] (blue).

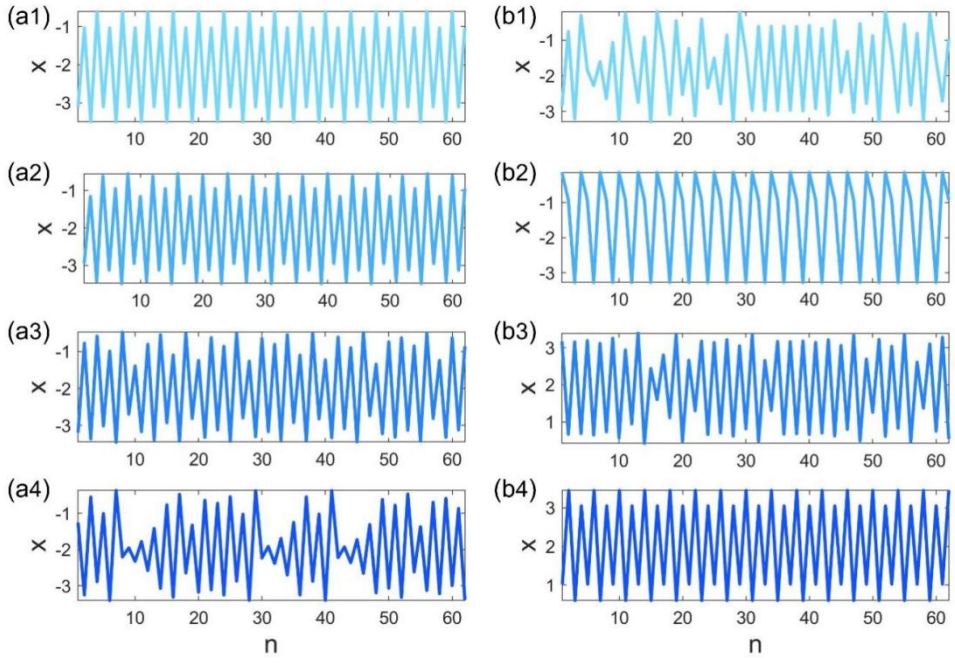

Figure 3. Dynamics of the neural map model for (a) $A = 8$ and (b) $A = 9$ by adding the memristor with different strengths. (a1,b1) $\mu = 0$, (a2,b2) $\mu = 0.02$, (a3,b3) $\mu = 0.05$, (a4,b4) $\mu = 0.1$. The initial condition is $[-1,0]$.

Another notable point is that the basin of attraction of coexisting attractors is dependent on the strength of the magnetic induction. In order to show this, two basins of attraction corresponding to the periodic (blue) and chaotic dynamics (red) is depicted in Figure 4. In part (a), $\mu = 0.1$, and in part (b), $\mu = 0.25$ is set. In smaller induction strengths, the basins are less dependent on ϕ_0. As induction strength increases, the basins change and have more relation with the initial condition of the magnetic flux variable. The coexisting dynamics of the model for $A = 8$ and for different μ values are shown in Figure 5. In parts (a)–(c), the value of μ is set to $\mu = 0.1$, $\mu = 0.2$, and $\mu = 0.51$. The left panel refers to the initial condition $[1,0]$, and the right to $[-1,0]$. For $\mu = 0.1$, a chaotic and a periodic pattern coexist, while for $\mu = 0.2$, two periodic dynamics with different patterns and periods coexist. By setting $\mu = 0.51$, the coexistence of period dynamics and a fixed point is observed.

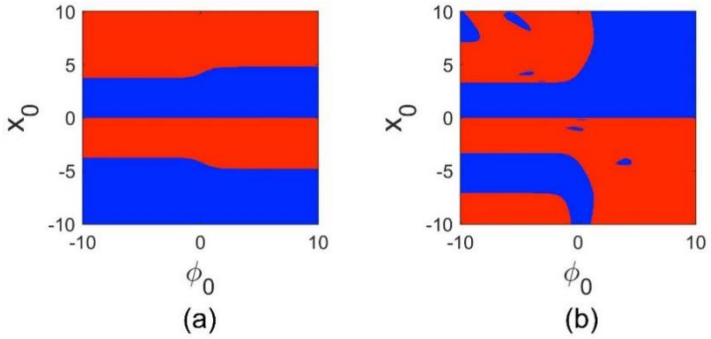

Figure 4. Basin of attraction of coexisting periodic (blue) and chaotic (red) dynamics in memristive neural map model for $A = 8$. (a) $\mu = 0.1$, (b) $\mu = 0.25$.

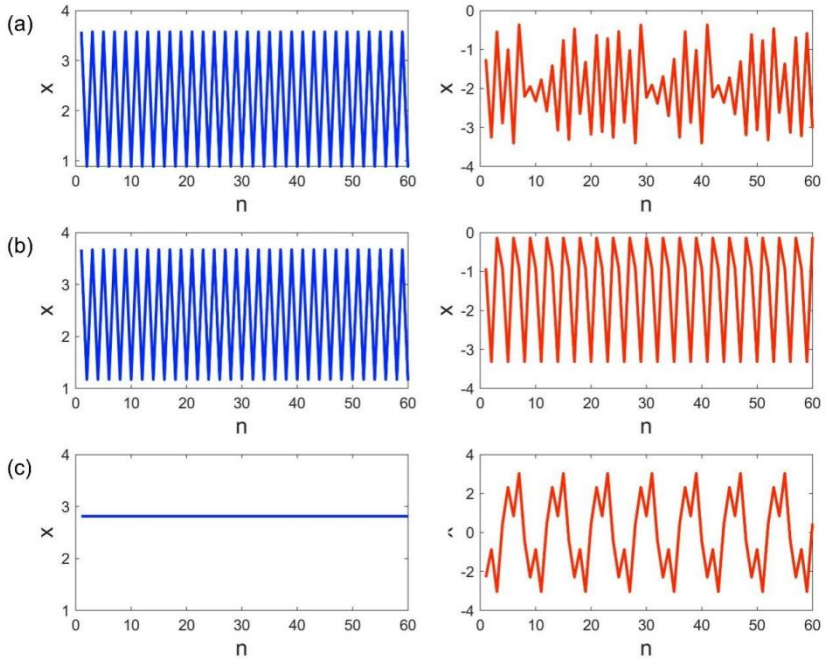

Figure 5. Coexisting dynamics of the memristive neural map model for A=8. (a) $\mu = 0.1$, (b) $\mu = 0.2$, (c) $\mu = 0.51$. The left and right panels show the time series corresponding to the initial conditions $[1,0]$ and $[-1,0]$, respectively.

4. Coupled memristive neural maps

In addition to the dynamics of the neural map model, the memristor can remarkably change the collective behavior of the coupled maps. A network of non-locally coupled neural maps can be described by,

$$x_i(n+1) = B\tanh(w_1 x_i(n)) - A\tanh(w_2 x_i(n)) + \mu\, x_i(n)\tanh\big(\phi_i(n)\big) + g_e \sum_{j=i-P}^{i+P} (x_j(n) - x_i(n)) + g_c(v_s - x_i(n)) \sum_{\substack{j=i-P, \\ i\neq j}}^{i+P} \frac{1}{1+\exp -\beta\big(x_j - \theta_s\big)}, \tag{5}$$

$$\phi_i(n+1) = \phi_i(n) + x_i(n) + g_m \sum_{j=i-P}^{i+P} (\phi_j(n) - \phi_i(n)), \quad i = 1, \dots, N, \;\; P = 10$$

where $N = 100$. The network is considered to be a ring of neural maps with non-local coupling where each map is connected to its $P = 10$ nearest neighbors from right and left. g_e, g_c, and g_m represent the coupling strength for the electrical, chemical, and magnetic coupling. The effect of each coupling type is investigated separately. Three different scenarios are considered: 1) the coupling is electrical ($g_c = g_m = 0$), 2) the coupling is magnetic ($g_e = g_c = 0$), 3) the coupling is chemical ($g_e = g_m = 0$). At first, the complete synchronization is examined by computing the numerical error:

$$E = < \frac{1}{(N-1)} \sum_{i=1}^{N} \sqrt{(x_i - x_1)^2} >_t \tag{6}$$

Besides the synchronization error, a statistical factor of synchronization (R) [57] is also computed which is based on the mean field theory, as follows:

$$F = \frac{1}{N}\sum_{i=1}^{N} x_i$$
$$R = \frac{< F^2 > - < F >^2}{\frac{1}{N}\sum_{i=1}^{N}(< x_i^2 > - < x_i >^2)} \tag{7}$$

where $<\cdot>$ denotes the time average. The synchronization can be detected when this synchronization factor is equal to 1.

The synchronization is investigated by varying μ and the coupling strength. The results for different coupling types are shown in Figure 6, where in the first row $P = 10$ and in the second row $P = 25$. The dark blue color indicates the synchronous area, and the black shows the instability. Figure 6(a1) represents the synchronization error by varying the electrical coupling strength ($g_m = g_c = 0$) for different μ values. There are some small synchronization regions in smaller coupling strengths. In part (b1), the magnetic coupling ($g_e = g_c = 0$) is examined. This figure has a synchronous area referring to very small μ values. In contrast to the two mentioned couplings, chemical coupling ($g_e = g_m = 0$)) results in a larger synchronization area (Figure 6(c1)). Consequently, it can be concluded that synchronization is achievable in wider regions of parameters

through chemical coupling. Comparing the first and the second rows shows that changing the network structure has a small impact on the results. By increasing P, the synchronization is still reached in a small area via electrical coupling (Figure 6(a2)). Moreover, the instability occurs in smaller couplings. In the case of magnetic coupling (Figure 6(b2)), increasing P has a small effect and the synchronization happens only in small μ values, and instability occurs in smaller couplings. For chemical coupling (Figure 6(c2)), the synchronization area is significantly larger than other couplings. Parts (d)–(f) of Figure 6 shows the synchronization factor R in red, computed for three coupling types and for $\mu = 0.5$. The synchronization error is also shown in blue color. It is seen that for electrical coupling, synchronization happens in a small region in $0.004 < g_e < 0.0095$. In contrast, for chemical coupling R factor equals 1 in $0.0005 < g_c < 0.0045$ and $0.021 < g_c < 0.05$ representing synchronization in larger area. In magnetic coupling, some coupling strength (g_m) results in $R = 1$, however the synchronization error is not zero. The reason is that in these coupling strength values, the systems are attracted by two fixed points. Hence, $R = 1$ do not represent complete synchronization.

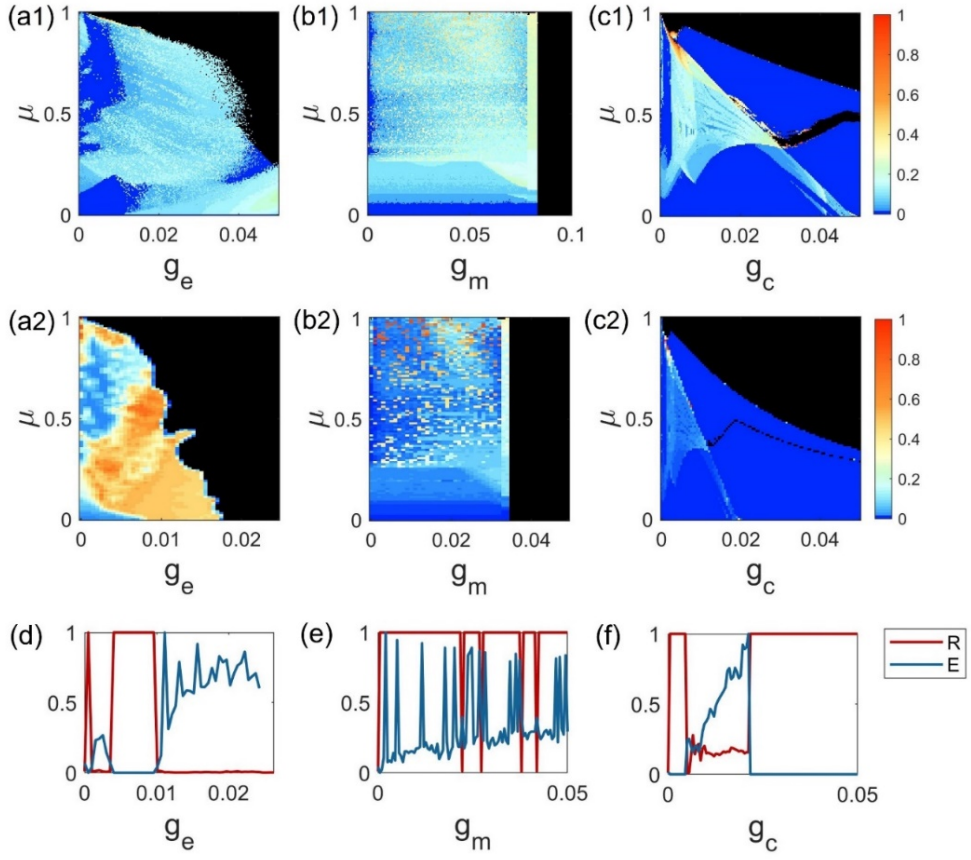

Figure 6. (a–c) The synchronization error of coupled memristive neural maps as a function of μ and coupling strength for (a) electrical coupling ($g_m = g_c = 0$), (b) magnetic coupling ($g_e = g_c = 0$), (c) chemical coupling ($g_e = g_m = 0$). The first and second rows correspond to two different network structures where in the first row $P = 10$ and in the second row $P = 25$. (d–f) The synchronization error (E) and the synchronization factor (R) as a function of coupling strength for $\mu = 0.5$. (d) electrical coupling, (e) magnetic coupling, (f) chemical coupling.

In the next step, we search for the collective behaviors in coupled maps before reaching complete synchrony. The initial conditions for the x state variables of all systems are set to $x(0) = -1$, while the initials of the ϕ are randomly chosen from [0 1]. In Figure 7, the map models are coupled with electrical coupling. In Figure 7(a), a chimera pattern is shown for $\mu = 0.4$ and $g_e = 0.007$. In this pattern, most systems are located in two clusters, and a few are not synchronous with the clusters. Figure 7(b) shows that while the synchronous clusters have periodic dynamics, the asynchronous systems are chaotic. For a bit stronger coupling, the asynchronous systems disappear and two clusters are formed. A two-cluster state is shown in Figure 7(c). The periodic time series of the clusters are shown in Figure 7(d).

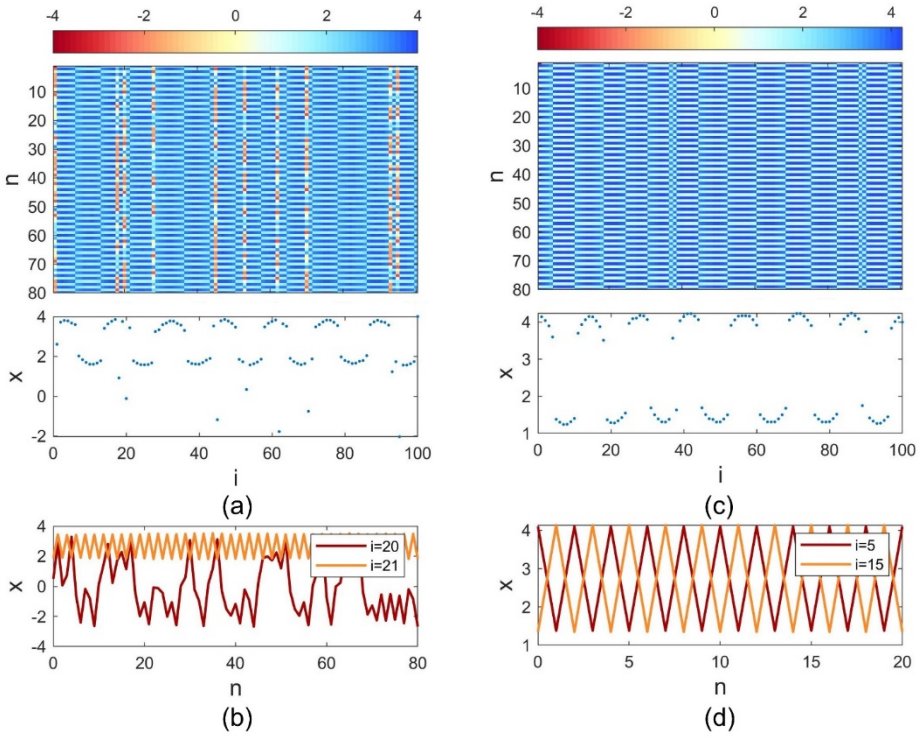

Figure 7. Dynamical behavior of electrically coupled neural map models (a) spatiotemporal pattern and the time snapshot for $\mu = 0.4$ and $g_e = 0.007$, (b) the corresponding time series of part (a). (c) spatiotemporal pattern and the time snapshot for $\mu = 0.4$ and $g_e = 0.009$, (d) the corresponding time series of part (c).

Figure 8 shows two cluster synchronization states when the systems are coupled with magnetic coupling. In part (a), the systems form four different clusters for $\mu = 0.1$ and $g_m = 0.03$; the time series are shown in part (b). By raising the coupling strength, four clusters are converted to two clusters. Figure 8(c) shows the pattern for $g_m = 0.08$ with the corresponding time series of the clusters shown in part (d). Figure 9 represents the network's magnetic coupling pattern for other μ values ($\mu = 0.5$). In this case, for low magnetic inductions, the systems are attracted by the fixed points, and oscillation death happens. Therefore, the pattern can be called chimera death (Figure 9(a)). The systems are returned to chaotic oscillating for larger induction strengths. Figure 9(c) shows an example of asynchronous chaotic oscillation for $g_m = 0.07$. The time series of the chaotic firing is shown in Figure 9(d).

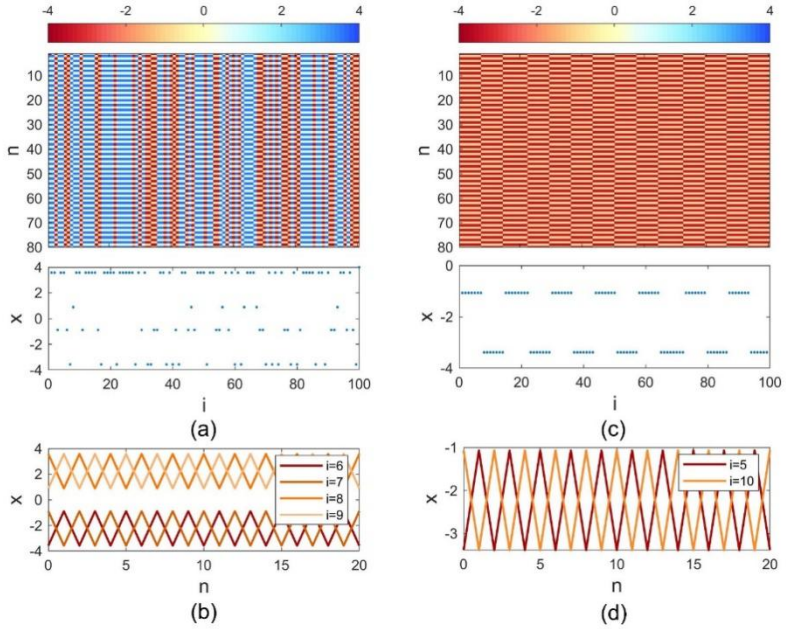

Figure 8. Dynamical behavior of magnetically coupled neural map models (a) spatiotemporal pattern and the time snapshot for $\mu = 0.1$ and $g_m = 0.03$, (b) the corresponding time series of part (a). (c) spatiotemporal pattern and the time snapshot for $\mu = 0.1$ and $g_m = 0.08$, (d) the corresponding time series of part (c).

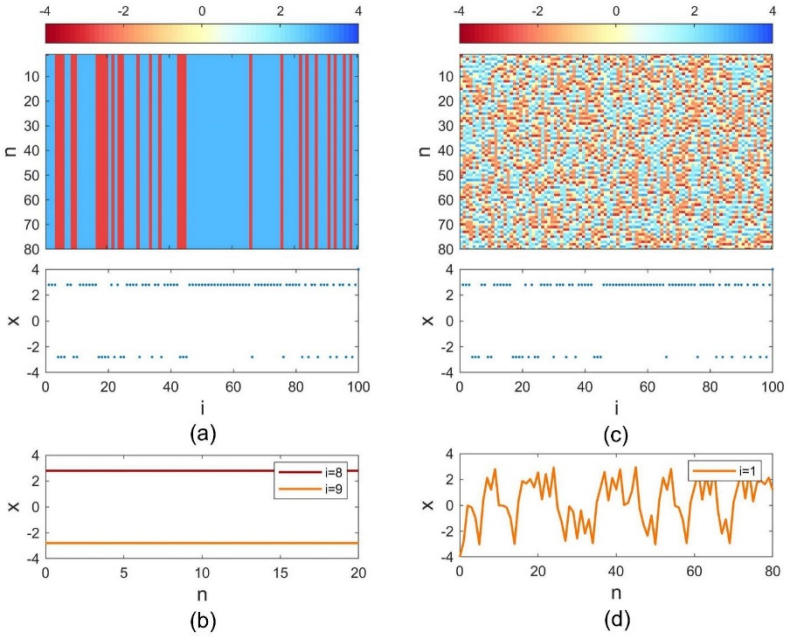

Figure 9. Dynamical behavior of magnetically coupled neural map models (a) spatiotemporal pattern and the time snapshot for $\mu = 0.5$ and $g_m = 0.04$, (b) the corresponding time series of part (a). (c) spatiotemporal pattern and the time snapshot for $\mu = 0.5$ and $g_m = 0.07$, (d) the corresponding time series of part (c).

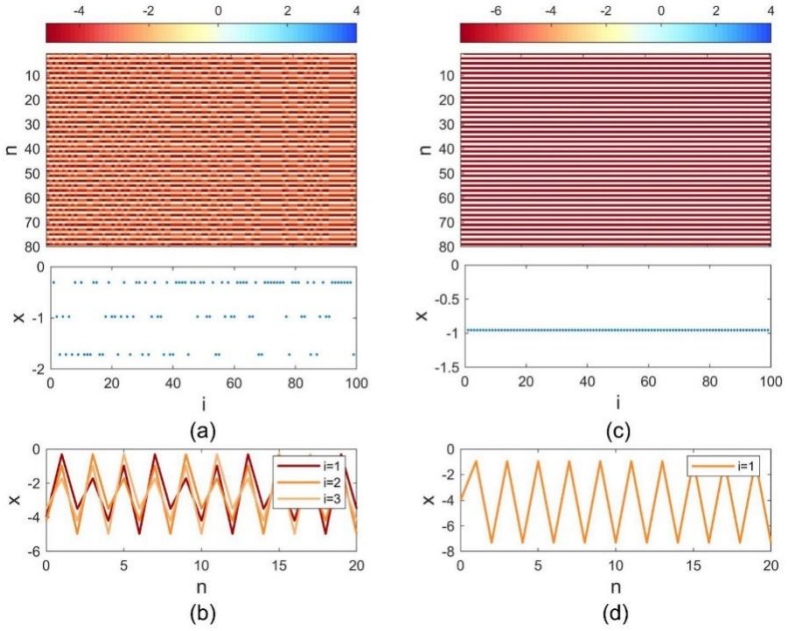

Figure 10. Dynamical behavior of chemically coupled neural map models (a) spatiotemporal pattern and the time snapshot for $\mu = 0.1$ and $g_c = 0.002$, (b) the corresponding time series of part (a). (c) spatiotemporal pattern and the time snapshot for $\mu = 0.1$ and $g_c = 0.005$, (d) the corresponding time series of part (c).

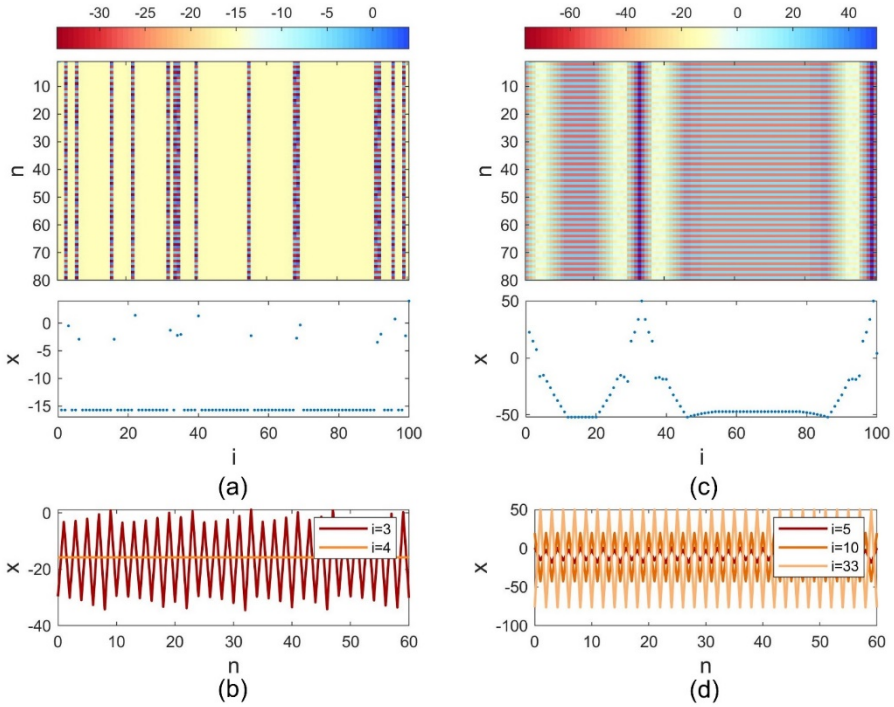

Figure 11. Dynamical behavior of chemically coupled neural map models (a) spatiotemporal pattern and the time snapshot for $\mu = 0.1$ and $g_c = 0.04$, (b) the corresponding time series of part (a). (c) spatiotemporal pattern and the time snapshot for $\mu = 0.4$ and $g_c = 0.03$, (d) the corresponding time series of part (c).

Finally, the patterns obtained with chemical coupling are shown in Figure 10. In Figure 10, μ is set to 0.1. In this case, for very small chemical coupling, synchronous clusters are organized (Figure 10(a),(b)). By slightly increasing the coupling, the systems are all synchronous, as shown in Figure 10(c) for $g_c = 0.005$, and have periodic behavior (Figure 10(d)). For stronger couplings, some of the systems are oscillating periodically, and some of them are attracted to a fixed point. An example of this state is shown in Figure 11(a),(b) for $g_c = 0.04$. Finally, by increasing the coupling, the systems are again synchronous and oscillate periodically. Other than the synchronous and cluster synchronous states, the chemically coupled systems can represent the chimera state. Figure 11(c) shows a chimera state for $\mu = 0.4$ and $g_c = 0.03$. It can be observed that there are synchronous and asynchronous groups. The time series corresponding to the synchronous and asynchronous groups are shown in Figure 11(d).

5. Conclusions

This paper presented a modified memristive neural map model using a hyperbolic memductance function. By introducing the memristor to a neuron model, the magnetic induction effects can be considered, which remarkably affect the model's behavior. Hence, in this paper, the dynamics of the neural model were investigated according to the magnetic induction strength. It was shown that varying the magnetic induction strength changes the dynamics, so its increment leads to the extension of multistable regions. The memristive model showed multistability in some parameter values where the original model was not multistable. Different regions' basins also varied as the magnetic induction was strengthened. The collective dynamics of the coupled memristive maps were also examined under electrical, chemical, and magnetic coupling. The behavior of the network was also under consideration in the asynchronized areas. The chimera state and the cluster synchronization state were observed for the electrical coupling and the chemical coupling. In contrast, cluster synchronization and chimera death states emerged for magnetic coupling. Finally, it was demonstrated that chemical coupling leads to a larger synchronization region. However, the considered chemical synapse contained a simplification of ignoring the time delay. We will consider the time delay and investigate its effects in our future work. Moreover, we assumed the network free of noise, which can affect the neural activities remarkably. For example, it can lead to occurrence of phenomena like coherence resonance [58,59]. In coherence resonance phenomenon, a specific noise intensity can lead to a maximized regularity in the network. In the future works, we will consider the proposed memristive model under noisy disturbance and study its impacts.

Use of AI tools declaration

The authors declare they have not used Artificial Intelligence (AI) tools in the creation of this article.

Acknowledgments

This work is partially funded by Centre for Nonlinear Systems, Chennai Institute of Technology, India vide funding number CIT/CNS/2023/RP/009, the Natural Science Foundation of China (No. 61901530, 62071496), the Natural Science Foundation of Hunan Province (No.2020JJ5767).

Conflict of interest

All authors declare no conflicts of interest in this paper.

References

1. M. Courbage, V. I. Nekorkin, Map based models in neurodynamics, *Int. J. Bifurcation Chaos*, **20** (2010), 1631–1651. https://doi.org/10.1142/S0218127410026733
2. B. Ibarz, J. M. Casado, M. A. Sanjuán, Map-based models in neuronal dynamics, *Phys. Rep.*, **501** (2011), 1–74. https://doi.org/10.1016/j.physrep.2010.12.003
3. A. Holko, M. Mędrek, Z. Pastuszak, K. Phusavat, Epidemiological modeling with a population density map-based cellular automata simulation system, *Expert Syst. Appl.*, **48** (2016), 1–8. https://doi.org/10.1016/j.eswa.2015.08.018
4. V. V. Tarasova, V. E. Tarasov, Logistic map with memory from economic model, *Chaos Solitons Fractals*, **95** (2017), 84–91. https://doi.org/10.1016/j.chaos.2016.12.012
5. K. Tanaka, T. Kinkyo, S. Hamori, Financial hazard map: Financial vulnerability predicted by a random forests classification model, *Sustainability*, **10** (2018), 1530. https://doi.org/10.3390/su10051530
6. Z. Hua, Y. Zhou, Exponential chaotic model for generating robust chaos, *IEEE Trans. Syst. Man Cybern.*, **51** (2019), 3713–3724. https://doi.org/10.1109/TSMC.2019.2932616
7. M. Ausloos, *The Logistic Map and the Route to Chaos: From the Beginnings to Modern Applications*, Springer Science & Business Media, 2006.
8. B. Cessac, B. Doyon, M. Quoy, M. Samuelides, Mean-field equations, bifurcation map and route to chaos in discrete time neural networks, *Physica D*, **74** (1994), 24–44. https://doi.org/10.1016/0167-2789(94)90024-8
9. Q. Xu, T. Liu, S. Ding, H. Bao, Z. Li, B. Chen, Extreme multistability and phase synchronization in a heterogeneous bi-neuron Rulkov network with memristive electromagnetic induction, *Cognit. Neurodyn.*, **17** (2023), 755–766. https://doi.org/10.1007/s11571-022-09866-3
10. I. Bashkirtseva, L. Ryashko, J. M. Seoane, M. A. Sanjuán, Noise-induced complex dynamics and synchronization in the map-based Chialvo neuron model, *Commun. Nonlinear Sci. Numer. Simul.*, **116** (2023), 106867. https://doi.org/10.1016/j.cnsns.2022.106867
11. J. Sausedo-Solorio, A. Pisarchik, Synchronization of map-based neurons with memory and synaptic delay, *Phys. Lett. A*, **378** (2014), 2108–2112. https://doi.org/10.1016/j.physleta.2014.05.003
12. I. Franović, V. Miljković, Power law behavior related to mutual synchronization of chemically coupled map neurons, *Eur. Phys. J. B*, **76** (2010), 613–624. https://doi.org/10.1140/epjb/e2010-00205-4
13. Q. Xu, T. Liu, C. T. Feng, H. Bao, H. G. Wu, B. C. Bao, Continuous non-autonomous memristive Rulkov model with extreme multistability, *Chin. Phys. B*, **30** (2021), 128702. https://doi.org/10.1088/1674-1056/ac2f30
14. S. He, K. Rajagopal, A. Karthikeyan, A. Srinivasan, A discrete Huber-Braun neuron model: From nodal properties to network performance, *Cognit. Neurodyn.*, **17** (2023), 301–310. https://doi.org/10.1007/s11571-022-09806-1

15. F. Wang, H. Cao, Mode locking and quasiperiodicity in a discrete-time Chialvo neuron model, *Commun. Nonlinear Sci. Numer. Simul.*, **56** (2018), 481–489. https://doi.org/10.1016/j.cnsns.2017.08.027
16. Y. Li, C. Li, Y. Zhao, S. Liu, Memristor-type chaotic mapping, *Chaos*, **32** (2022). https://doi.org/10.1063/5.0082983
17. X. Zhang, C. Li, E. Dong, Y. Zhao, Z. Liu, A conservative memristive system with amplitude control and offset boosting, *Int. J. Bifurcation Chaos*, **32** (2022), 2250057. https://doi.org/10.1142/S0218127422500572
18. Y. Jiang, C. Li, C. Zhang, Y. Zhao, H. Zang, A double-memristor hyperchaotic oscillator with complete amplitude control, *IEEE Trans. Circuits Syst. I*, **68** (2021), 4935–4944. https://doi.org/10.1109/TCSI.2021.3121499
19. H. Jeong, L. Shi, Memristor devices for neural networks, *J. Phys. D*, **52** (2018), 023003. https://doi.org/10.1088/1361-6463/aae223
20. D. B. Strukov, G. S. Snider, D. R. Stewart, R. S. Williams, The missing memristor found, *Nature*, **453** (2008), 80–83. https://doi.org/10.1038/nature06932
21. H. Wang, C. L. Li, S. Banerjee, S. B. He, Novel memristor and memristor-based applications, *Eur. Phys. J. Spec. Top.*, **231** (2022), 2973–2977. https://doi.org/10.1140/epjs/s11734-022-00697-1
22. M. Ge, Y. Jia, Y. Xu, L. Yang, Mode transition in electrical activities of neuron driven by high and low frequency stimulus in the presence of electromagnetic induction and radiation, *Nonlinear Dyn.*, **91** (2018), 515–523. https://doi.org/10.1007/s11071-017-3886-2
23. S. P. Adhikari, C. Yang, H. Kim, L. O. Chua, Memristor bridge synapse-based neural network and its learning, *IEEE Trans. Neural Networks Learn. Syst.*, **23** (2012), 1426–1435. https://doi.org/10.1109/TNNLS.2012.2204770
24. J. C. Magee, C. Grienberger, Synaptic plasticity forms and functions, *Ann. Rev. Neurosci.*, **43** (2020), 95–117. https://doi.org/10.1146/annurev-neuro-090919-022842
25. C. Chen, F. Min, Y. Zhang, B. Bao, Memristive electromagnetic induction effects on Hopfield neural network, *Nonlinear Dyn.*, **106** (2021), 2559–2576. https://doi.org/10.1007/s11071-021-06910-5
26. S. Hu, Y. Liu, Z. Liu, T. Chen, J. Wang, Q. Yu, et al., Associative memory realized by a reconfigurable memristive Hopfield neural network, *Nat. Commun.*, **6** (2015), 7522. https://doi.org/10.1038/ncomms8522
27. K. Rajagopal, A. Karthikeyan, S. Jafari, F. Parastesh, C. Volos, I. Hussain, Wave propagation and spiral wave formation in a Hindmarsh-Rose neuron model with fractional-order threshold memristor synapse, *Int. J. Mod. Phys. B*, **34** (2020), 2050157. https://doi.org/10.1142/S021797922050157X
28. Q. Xu, Z. Ju, S. Ding, C. Feng, M. Chen, B. Bao, Electromagnetic induction effects on electrical activity within a memristive Wilson neuron model, *Cognit. Neurodyn.*, **16** (2022), 1221–1231. https://doi.org/10.1007/s11571-021-09764-0
29. S. Qiao, C. Gao, Complex dynamics of a non-smooth temperature-sensitive memristive Wilson neuron model, *Commun. Nonlinear Sci. Numer. Simul.*, **125** (2023), 107410. https://doi.org/10.1016/j.cnsns.2023.107410
30. C. Li, Y. Yang, X. Yang, Y. Lu, Application of discrete memristors in logistic map and Hindmarsh-Rose neuron, *Eur. Phys. J. Spec. Top.*, **231** (2022), 3209–3224. https://doi.org/10.1140/epjs/s11734-022-00645-z

31. Q. Lai, C. Lai, H. Zhang, C. Li, Hidden coexisting hyperchaos of new memristive neuron model and its application in image encryption, *Chaos Solitons Fractals*, **158** (2022), 112017. https://doi.org/10.1016/j.chaos.2022.112017
32. C. Gao, S. Qiao, X. An, Global multistability and mechanisms of a memristive autapse-based Filippov Hindmash-Rose neuron model, *Chaos Solitons Fractals*, **160** (2022), 112281. https://doi.org/10.1016/j.chaos.2022.112281
33. S. Qiao, C. Gao, X. An, Hidden dynamics and control of a Filippov memristive hybrid neuron model, *Nonlinear Dyn.*, **111** (2023), 10529–10557. https://doi.org/10.1016/j.chaos.2022.112017
34. A. Arenas, A. Díaz-Guilera, J. Kurths, Y. Moreno, C. Zhou, Synchronization in complex networks, *Phys. Rep.*, **469** (2008), 93–153. https://doi.org/10.1016/j.physrep.2008.09.002
35. Z. Wang, R. Ramamoorthy, X. Xi, H. Namazi, Synchronization of the neurons coupled with sequential developing electrical and chemical synapses, *Math. Biosci. Eng.*, **19** (2022), 1877–1890. https://doi.org/10.3934/mbe.2022088
36. S. N. Chowdhury, S. Majhi, M. Ozer, D. Ghosh, M. Perc, Synchronization to extreme events in moving agents, *New J. Phys.*, **21** (2019), 073048. https://doi.org/10.1088/1367-2630/ab2a1f
37. G. Vivekanandhan, H. Natiq, Y. Merrikhi, K. Rajagopal, S. Jafari, Dynamical analysis and synchronization of a new memristive Chialvo neuron model, *Electronics*, **12** (2023), 545. https://doi.org/10.3390/electronics12030545
38. S. He, Complexity and chimera states in a ring-coupled fractional-order memristor neural network, *Front. Appl. Math. Stat.*, **6** (2020), 24. https://doi.org/10.3389/fams.2020.00024
39. Z. Wang, H. Tian, O. Krejcar, H. Namazi, Synchronization in a network of map-based neurons with memristive synapse, *Eur. Phys. J. Spec. Top.*, **231** (2022), 4057–4064. https://doi.org/10.1140/epjs/s11734-022-00691-7
40. F. Parastesh, S. Jafari, H. Azarnoush, Z. Shahriari, Z. Wang, S. Boccaletti, et al., Chimeras, *Phys. Rep.*, **898** (2021), 1–114. https://doi.org/10.1016/j.physrep.2020.10.003
41. S. Majhi, B. K. Bera, D. Ghosh, M. Perc, Chimera states in neuronal networks: A review, *Phys. Life Rev.*, **28** (2019), 100–121. https://doi.org/10.1016/j.plrev.2018.09.003
42. I. Franović, K. Todorović, N. Vasović, N. Burić, Cluster synchronization of spiking induced by noise and interaction delays in homogenous neuronal ensembles, *Chaos*, **22** (2012). https://doi.org/10.1063/1.4753919
43. I. Franović, K. Todorović, N. Vasović, N. Burić, Spontaneous formation of synchronization clusters in homogenous neuronal ensembles induced by noise and interaction delays, *Phys. Rev. Lett.*, **108** (2012), 094101. https://doi.org/10.1103/PhysRevLett.108.094101
44. M. Mehrabbeik, F. Parastesh, J. Ramadoss, K. Rajagopal, H. Namazi, S. Jafari, Synchronization and chimera states in the network of electrochemically coupled memristive Rulkov neuron maps, *Math. Biosci. Eng.*, **18** (2021), 9394–9409. https://doi.org/10.3934/mbe.2021462
45. K. Li, B. Bao, J. Ma, M. Chen, H. Bao, Synchronization transitions in a discrete memristor-coupled bi-neuron model, *Chaos Solitons Fractals*, **165** (2022), 112861. https://doi.org/10.1016/j.chaos.2022.112861
46. B. Ramakrishnan, M. Mehrabbeik, F. Parastesh, K. Rajagopal, S. Jafari, A new memristive neuron map model and its network's dynamics under electrochemical coupling, *Electronics*, **11** (2022), 153. https://doi.org/10.3390/electronics11010153

47. S. Wang, Z. Wei, Synchronization of coupled memristive Hindmarsh–Rose maps under different coupling conditions, *AEU-Int. J. Electron. Commun.*, **161** (2023), 154561. https://doi.org/10.1016/j.aeue.2023.154561
48. G. Baghdadi, S. Jafari, J. C. Sprott, F. Towhidkhah, M. H. Golpayegani, A chaotic model of sustaining attention problem in attention deficit disorder, *Commun. Nonlinear Sci. Numer. Simul.*, **20** (2015), 174–185. https://doi.org/10.1016/j.cnsns.2014.05.015
49. B. Bao, H. Qian, Q. Xu, M. Chen, J. Wang, Y. Yu, Coexisting behaviors of asymmetric attractors in hyperbolic-type memristor based Hopfield neural network, *Front. Comput. Neurosci.*, **11** (2017), 81. https://doi.org/10.3389/fncom.2017.00081
50. D. Ding, J. Luo, X. Shan, Y. Hu, Z. Yang, L. Ding, Coexisting behaviors of a fraction-order novel hyperbolic-type memristor Hopfield neuron network based on three neurons, *Int. J. Mod. Phys. B*, **34** (2020), 2050302. https://doi.org/10.1142/S0217979220503026
51. R. Li, Z. Wang, E. Dong, A new locally active memristive synapse-coupled neuron model, *Nonlinear Dyn.*, **104** (2021), 4459–4475. https://doi.org/10.1007/s11071-021-06574-1
52. K. Li, H. Bao, H. Li, J. Ma, Z. Hua, B. Bao, Memristive Rulkov neuron model with magnetic induction effects, *IEEE Trans. Ind. Inf.*, **18** (2021), 1726–1736. https://doi.org/10.1109/TII.2021.3086819
53. S. Garai, S. Karmakar, S. Jafari, N. Pal, Coexistence of triple, quadruple attractors and Wada basin boundaries in a predator-prey model with additional food for predators, *Commun. Nonlinear Sci. Numer. Simul.*, **121** (2023), 107208. https://doi.org/10.1016/j.cnsns.2023.107208
54. Y. Zhou, J. Gao, K. D. White, I. Merk, K. Yao, Perceptual dominance time distributions in multistable visual perception, *Biol. Cybern.*, **90** (2004), 256–263. https://doi.org/10.1007/s00422-004-0472-8
55. D. Durstewitz, G. Deco, Computational significance of transient dynamics in cortical networks, *Eur. J. Neurosci.*, **27** (2008), 217–227. https://doi.org/10.1111/j.1460-9568.2007.05976.x
56. T. Ionescu, Exploring the nature of cognitive flexibility, *New Ideas Psychol.*, **30** (2012), 190–200. https://doi.org/10.1016/j.newideapsych.2011.11.001
57. Y. Xu, Y. Jia, J. Ma, A. Alsaedi, B. Ahmad, Synchronization between neurons coupled by memristor, *Chaos Solitons Fractals*, **104** (2017), 435–442. https://doi.org/10.1016/j.chaos.2017.09.002
58. P. Zhou, Y. Xu, J. Ma, Dynamical and coherence resonance in a photoelectric neuron under autaptic regulation, *Physica A*, **620** (2023), 128746. https://doi.org/10.1016/j.physa.2023.128746
59. A. N. Pisarchik, A. E. Hramov, Coherence resonance in neural networks: Theory and experiments, *Phys. Rep.*, **1000** (2023), 1–57. https://doi.org/10.1016/j.physrep.2022.11.004

AIMS Press